Hints of Nonhierarchical Folding of Acidic Fibroblast Growth Factor†

Jesús M. Sanz,*,‡,§ M. Angeles Jiménez,|| and Guillermo Giménez-Gallego*,‡

Departamento de Estructura y Función de Proteínas, Centro de Investigaciones Biológicas (CSIC), and Instituto de Quømica-Føsica Rocasolano (CSIC), Madrid, Spain

Received September 10, 2001; Revised Manuscript Received November 14, 2001

ABSTRACT: We have analyzed by circular dichroism (CD) and proton nuclear magnetic resonance (NMR) the helical propensity of the all-β protein acidic fibroblast growth factor (aFGF) and two peptides corresponding to β-strand 8 (β8 peptide, amino acids 95−107) and the β-strand 8/turn/β-strand 9 hairpin (β8/9 peptide, amino acids 95−114), which has been involved in receptor binding. A secondary structure prediction of aFGF carried out by several procedures labels the 95−104 sequence as predominantly α-helical. A titration of aFGF with 2,2,2-trifluoroethanol (TFE) induces a change in the far-UV CD spectrum of the protein giving rise to a prominent α-helical shape (22% α-helix). The cooperativity of the transition and the moderate TFE concentrations used (midpoint at 24%) suggest that the effect of TFE is specific. Moreover, a titration performed at pH 2 yields a higher amount of α-helix (55%) at a smaller TFE concentration. Synthetic peptides containing the β8 and β8/9 sequences display a random coil conformation at pH 7 but acquire α-helical structure in the presence of TFE, methanol, and SDS micelles. At pH below 3.0 a significant amount (20−30%) of α-helical conformation is present in both the β8 and β8/9 peptides even in the absence of other solvent additives. The secondary structure of the peptides was determined by proton nuclear magnetic resonance (^{1}H NMR). These results suggest that the 95−114 sequence of aFGF has helical propensity and that the protein may fold nonhierarchically in the early steps of folding, acquiring its final β-structure by a later interaction with the rest of the polypeptide.

A considerable amount of work has allowed to establish several models that aim to explain the steps followed by a polypeptide chain to acquire its final, native structure. Some sequential models (*1*−*3*) assume that intermediate states accumulate in a well-defined folding pathway and are built up of nativelike secondary structure segments that are stabilized by nonspecific hydrophobic interactions (the "molten globule" state). Other sequential models (*4*) consider that the formation of secondary structure is preceded by a hydrophobic collapse of the nonpolar side chains. In the nucleation−condensation mechanism (*5*) the formation of the nucleus and of the secondary structure is a concerted event for small proteins or units (foldons), and larger proteins, built up from such foldons, fold in parts. Finally, in the "funnel" model (*6*) there is no single pathway but a multiple set of parallel microscopic pathways. In most cases, these theoretical mechanisms describe folding as a strongly hierarchical process in which only nativelike intermediate structures are significant whereas "misfolded" structures are considered "off-pathway".

Whereas the hierarchical model has been sucessful in explaining the folding of several all-α and mixed α/β proteins, it does not provide a satisfactory explanation of the folding of all-β proteins, where local formation of a β-strand depends on long-range interactions with another (preformed) β-strand. In this sense, the studies of all-β proteins are only very recent, and little is known of the early steps of their folding (*7*). However, some of these studies seem to undermine the notion of hierarchical folding as a general feature. For example, the far-ultraviolet circular dichroism (far-UV CD) spectrum of acid-denatured retinoic acid binding protein displays a larger amount of α-helix than in the native state (*8*). Moreover, kinetic studies on the folding of β-lactoglobulin monitored by stopped-flow CD show the formation of a transient α-helical intermediate in the millisecond time scale (*9, 10*). The structure of this kinetic intermediate correlates with the propensity of β-lactoglobulin to form α-helix in equilibrium in mild denaturing conditions (*11*) and in the presence of 2,2,2-trifluoroethanol (TFE)[1] (*12*). Furthermore, peptides corresponding to the sequences of β-strands of β-lactoglobulin that are initially predicted as α-helix show some helical character in TFE/water solutions (*13*). The induction of helix by TFE, especially at moderate concentrations (<40%), seems specific, since the existence of a linear correlation between [TFE] and the amount of helix predicted from the amino acid sequence has been shown (*12*). The predicted helix percentage is often very different from that found in the native state (*12*).

† J.M.S. was a recipient of a Contrato de Reincorporación from the Spanish Ministerio de Educación y Ciencia. This work was partially funded by the Dirección General de Investigación Científica y Técnica and by the Fundación Gregorio Marañón-Boehringer Ingelheim S.A. and the Fundación Futuro-Boehringer Ingelheim S.A.

* Corresponding authors. J.M.S.: Centro de Biología Molecular y Celular, Universidad Miguel Hernández, Av. Ferrocarril s/n, Elche 03202, Spain. Tel: (34)966658460. Fax: (34)966658758. E-mail: jmsanz@umh.es. G.G.-G.: Centro de Investigaciones Biológicas (CSIC), Velázquez 144, Madrid 28006, Spain; Tel: (34)915611800. Fax: (34)915627518. E-mail: gimenez.gallego@cib.csic.es.

‡ Centro de Investigaciones Biológicas (CSIC).

§ Present address: Centro de Biología Molecular y Celular, Universidad Miguel Hernández, Elche, Spain.

|| Instituto de Quømica-Føsica Rocasolano (CSIC).

[1] Abbreviations: TFE, 2,2,2-trifluoroethanol; aFGF, acidic fibroblast growth factor; NPN, *N*-phenyl-1-naphthylamine; ANS, 1-anilino-8-naphthalenesulfonic acid.

10.1021/bi0157619 CCC: $22.00
Published on Web 01/16/2002

The acquisition of different conformations by the same polypeptidic sequence is a subject of increasing attention. Zhong and Johnson (*14*) showed that the same sequence can be found in α-helix, β-strand, and random coil conformations depending on the characteristics of the solvent. On the other hand, Minor and Kim (*15*) have designed a "chameleon" peptide that folds as an α-helix or a β-strand when placed in different positions of the sequence of the immunoglobulin-binding domain of protein G. An important consequence of these phenomena is that a shift to non-native conformations may trigger the development of some pathologies such as Alzheimer's disease, transimisible encephalopathies, and fatal amyloidoses [see, e.g., reviews by Thomas et al. (*16*) and Carrell and Lomas (*17*)].

Acidic fibroblast growth factor (aFGF) is an all-β protein with a wide range of functionalities including the induction of cell proliferation, effect on cell differentiation, and other hormone-like activities such as hypotensive response (*18*). The mitogenic activity of aFGF is mediated by the binding of the anionic polysaccharide heparin (*19*, *20*) or *myo*-inositol hexasulfate (*21*). These two ligands protect aFGF against denaturation (*21*, *22*). The three-dimensional structure of aFGF has been solved both by X-ray crystallography (*23*, *24*) and proton nuclear magnetic resonance spectroscopy (^{1}H NMR) (*21*, *25*). The protein folds according to a β-trefoil topology (*26*) with six β-strand pairs, three of which form a six-stranded β-barrel structure. The β structure of aFGF accounts for 50% of the overall structure, the rest being turns and nonregular structure. There are no traces of α-helix. Due to its pharmacological application, the study of the folding of aFGF is of special interest. In this sense, we have characterized a structured intermediate of the protein that accumulates at pH 4.0 (*27*). This intermediate possibly retains a high amount of the nativelike secondary structure and the hydrophobic core and is also capable of interacting with liposomes, a fact that may be related to its competency for membrane translocation (*27*).

In this paper, we have investigated the possible existence of non-native conformations of aFGF in order to gain a deeper insight into the folding pathway of the protein.

EXPERIMENTAL PROCEDURES

Materials. *N*-Phenyl-1-naphthylamine (NPN), dimyristoylglycerophosphocholine, and 2,2,2-trifluoroethanol were purchased from Sigma. Purified peptides β8 (Ac-EEALFLERLEENH-NH_2) and β8/9 (Ac-EEALFLERLEENHYNTYISK-NH_2) were purchased from Chiron Mimotopes Pty. Ltd.

Protein Preparation. Chymotrypsin-digested aFGF (residues 23−154) was obtained as previously described (*21*). Protein concentration was estimated spectrophotometrically using an extinction coefficient $E^{0.1\%} = 1.26$.

Fluorescence. Fluorescence experiments were carried out in a Perkin-Elmer LS-50B spectrofluorometer. For intrinsic fluorescence experiments, the protein concentration was 1 or 15 μM, where no inner filter effects are present. The excitation wavelength was 280 nm, and the excitation and emission slits were 2.5 and 10 nm, respectively. Buffers (50 mM) were HCl (pH 1.0−2.0), glycine (pH 2.2−3.6), acetate (pH 3.8−5.6), and phosphate (pH 5.8−7.5) plus 50 mM NaCl. The pH of the samples was measured directly on a Unifet pH meter after the measurements.

For *N*-phenyl-1-naphthylamine fluorescence experiments, the concentrations of protein and probe were both 1 μM, the excitation wavelength was set to 340 nm, and the excitation and emission slits were 5 nm.

Circular Dichroism. CD experiments were carried out in a Jasco J-720 spectropolarimeter fitted with a thermostated cell holder and interfaced with a Neslab RTE-110 water bath. Isothermal wavelength spectra were acquired at a scan speed of 50 nm/min and averaged over at least six scans. The response time was 2 s. Ellipticities ([θ]) are expressed in units of deg cm^2 dmol^{-1} using the mean residue concentration. Buffers used were the same as described above for fluorescence experiments. α-Helical secondary structure content was calculated from far-UV CD traces using the equation (*28*):

$$f_\alpha = \frac{[\theta]_{222}^{exp} - [\theta]_{222}^{coil}}{[\theta]_{222}^{max} - [\theta]_{222}^{coil}} \quad (1)$$

where f_α is the fraction of α-helix, $[\theta]_{222}^{exp}$ is the experimental value of the ellipticity at 222 nm, $[\theta]_{222}^{coil}$ is the ellipticity value of a random coil spectrum (calculated as $[\theta]_{222}^{coil} = 2220 - 53t$, with t being the temperature in centigrade), and $[\theta]_{222}^{max}$ is the ellipticity expected for a 100% helical peptide [calculated as $[\theta]_{222}^{max} = (-44000 + 250t)(1 - 3/N_r)$, with N_r being the number of residues].

TFE transitions were analyzed, when appropriate, with the binding-exchange model of Jasanoff and Fersht (*29*):

$$\Delta G(\text{TFE}) = \Delta G(H_2O) - m([\text{TFE}]/[H_2O]) \quad (2)$$

where ΔG(TFE) is the stabilization free energy in the presence of TFE, $\Delta G(H_2O)$ is the energy in absence of TFE, and m is a constant.

pH titrations were analyzed with the equation (*30*):

$$[\theta]_{222} = \frac{[\theta]_{222}^{H} + [\theta]_{222}^{L} 10^{-m_{eq}(pH - MP_{eq})}}{1 + 10^{-m_{eq}(pH - MP_{eq})}} \quad (3)$$

where $[\theta]_{222}^{H}$ is the ellipticity value at higher pH, $[\theta]_{222}^{L}$ is the value at lower pH, m_{eq} is the number of protons taken up in the pH-induced transition, and MP_{eq} is the equivalence midpoint.

Finally, the expected $[\theta]_{222}$ in 40% TFE was calculated from the predicted percentage of helix by using the equations:

$$[\theta]_{222}(40\%\ \text{TFE, pH 2}) = -13200 - 210\,(\%\ \text{predicted helix}) \quad (4)$$

$$[\theta]_{222}(40\%\ \text{TFE, pH 6}) = -8770 - 225\,(\%\ \text{predicted helix}) \quad (5)$$

These equations were derived by plotting the experimental ellipticity at 222 nm observed at 40% TFE and different pH values for 23 proteins versus the percentage of predicted helix according to a joint prediction method (*12*).

Nuclear Magnetic Resonance. NMR samples were prepared by dissolving the peptide in 0.5 mL of 20 mM phosphate buffer, pH 2.0/D_2O (9:1 ratio by volume). The appropiate amount of 2,2,2-trifluoroethanol-d_3 (Cambridge Isotope Laboratories) was added to the aqueous solution. The aFGF concentration was 0.1 mM, whereas peptide concen-

```
           23                                     50                         75
           |  β1        β2          β3  |              β4        β5      |  β6          β7
            ------>  ------>   ------>            ------>   ------>   ------>   ----->
aFGF       KKPKLLYCSNGGHFLRILPDGTVDGTRDRSDQHIQLQLSAESVGEVYIKSTETGQYLAMDTDGLLYGSQT
DSC        cccceeeeccccceeeeecccceeeeecccccceeeeeecccccеeeeecccccеeeeecccceeecccc
GOR4       ccceeeeeccccceeeecccccccccccccchhhhhhhhhhhccceeeeeccccceeeecccccеeeeccc
HNNC       ccceeeeeccccceeeeeccccccccccchhhheeeeecccccceeeeeeccccceeeecccceeecccc
PHD        ccceeeeecccceeeeecccccccccccccccceeeeeeeecceeeeeeecccеeeeeeccccеeeeecc
Predator   ccceeeeecccceeeeecccccеeeecccccccccеeeeeccccеeeeeecccccеeeecccccеeeecc
SIMPA96    ccceeeeecccceeeeeccccccccccccccchhhhhhhhhcccceeeeeccccceeeeecccceeecccc
SOPMA      ccceeeeetttceeeeecttcceeccccccccchheeeehhhctteeeeetcctteeeeectttceeeccc

              100                        125                             154
               |β8        β9         β10|    β11              β12       |
             ------>   ------>      ------>  ---->           ------>
aFGF       PNEECLFLERLEENHYNTYISKKHAEKNWFVGLKKNGSCKRGPRTHYGQKAILFLPLPVSSD
DSC        cccceeeeeeccccccceeeeecccccccеeeeccccccccccccccccceeeecccccccc
GOR4       ccchhhhhhhhcccccceeeeecccceeeeeeeccccccccccccccccеeeeeecccеeec
HNNC       cchhhhhhhhhhhhcccchееccccccceeeeeccccccccccccccccеeeeeeecccccc
PHD        ccchhhheehhhccccceeeeeeccceeeeeeeccccccccccccccccеeeeeeccccccc
Predator   cccccceeeeeccccceeeeeccccccccccccccccccccccccccccccccеeeeecccc
SIMPA96    cchhhhhhhhhhhcccceeeccccccccеeeeecccccccccccccccccеeeeeeeccccc
SOPMA      ccchhhhhhhhhhttchheehcccccccеeeeecttccccccccccccccеeeeeccccccc
```

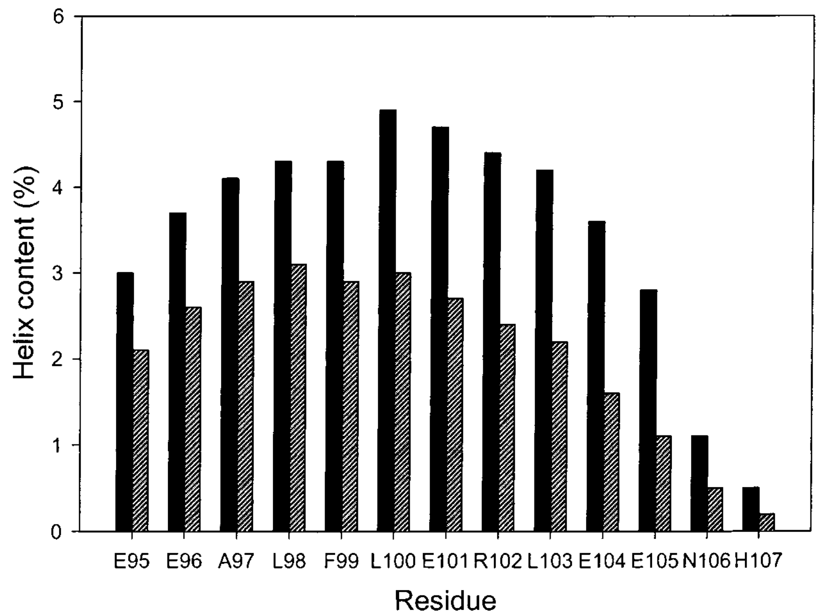

FIGURE 1: Secondary structure prediction for aFGF. Upper panel: predictions were carried out by several methods using the NPSA server as described in Experimental Procedures. Key: h, helix prediction; **e**, extended (β) prediction; t, turn prediction; c, coil prediction. Only SOPMA performs turn predictions. Native aFGF β-strands are highlighted in bold and represented by arrows. Lower panel: AGADIR prediction for the β8 peptide on a per residue level at pH 2.0 (black bars) and pH 7.0 (hatched bars).

trations were about 1 mM. pH was measured with a glass microelectrode and was not corrected for isotope effects. The temperature of the NMR probe was calibrated using a methanol sample. Sodium 3-trimethylsilyl[2,2,3,3-$^2H_4$]-propionate (TSP) was used as an internal reference. NMR experiments were performed on a Bruker AMX-600 spectrometer. Phase-sensitive two-dimensional COSY (*31*), TOCSY (*32*), NOESY (*33*), and ROESY (*34*, *35*) spectra were recorded by standard techniques using presaturation of the water signal and the time-proportional phase incrementation mode (*36*). Mixing times of 200 and 150 ms were used for NOESY and ROESY spectra, respectively. TOCSY spectra were recorded using a MLEV17 spin-lock sequence with a z filter (*37*) and a 80 ms mixing time. Acquisition data matrices were defined by 2018 $\times$ 512 points in t_2 and t_1, respectively. Data were processed using the standard XWIN NMR Bruker program on a Silicon Graphics computer. The 2D data matrix was multiplied by a square-sine-bell window function with the corresponding shift optimized for every spectrum and zero-filled to a 4K $\times$ 1K complex matrix prior to Fourier transformation. Baseline correction was applied in both dimensions.

Lipid Preparation. Small unilamellar vesicules were prepared by dissolving the solid phospholipid (dimyristoylglycerophosphocholine) in chloroform followed by evaporation to dryness under nitrogen. The lipid film was suspended in the corresponding buffer and sonicated in a Branson 1210 bath-type sonicator until optical clarity. The solution was finally centrifuged for 5 min at 14000 rpm prior to use and stored for at most 6 h on ice.

Protein Secondary Structure Prediction. Predictions were carried out at the Network Protein Sequence Analysis (NPSA

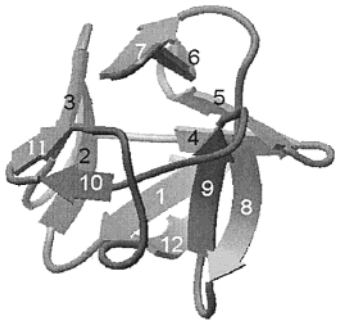

FIGURE 2: Localization of the β8/9 hairpin in the three-dimensional structure of aFGF. The picture was drawn using WebLab Viewer (Molecular Simulations Inc.).

server, Université Claude-Bernard and Centre Nationale de la Recherche Scientifique) (http://npsa-pbil.ibcp.fr). Methods selected were DSC (*38*), GOR4 (*39*), HNNC (*40*), PHD (*41*), PREDATOR (*42*), SIMPA96 (*43*), and SOPMA (*44*). AGADIR prediction (*45*) was carried out at the web address http://www.embl-heidelberg.de/Services/serrano/agadir/agadir-start.html.

RESULTS

Secondary Structure Prediction for aFGF. A secondary structure prediction was run for aFGF using the NPSA server, as described in Experimental Procedures (Figure 1). The overall prediction of β-strands and loops fits nicely to the experimental data, except in the cases of β-strand 4 (mixed α and β predictions); β-strands 3 and 11, where the loop prediction outweights the β prediction; and β-8, where there is a noteworthy α-helix prediction with a high degree of consensus between the methods tested. β-Strand 8, together with β-strand 9, forms one of the three hairpins that constitute the basic structure of the β-barrel in aFGF (Figure 2), and it participates in the binding to the membrane receptor through hydrophobic and van der Waals interactions involving Leu-103, Tyr-108, and the main chain atoms linking Glu-104 and Glu-105, as well as hydrogen bonds from the side chains of His-93 and Asn-95 and an ion pair involving Glu-101 (*46*).

Effect of TFE on the Structure of aFGF. Since there are some regions of aFGF that are predicted to have α-helical propensity, we have investigated such tendency in the presence of 2,2,2-trifluoroethanol (TFE) by circular dichroism (CD). TFE has been shown to be a secondary structure enhancer, especially for local propensities such as α-helix but also for β structures (see ref *47* for an extensive review). The far-UV CD spectrum of native aFGF at pH 7.0 is shown in Figure 3A. It displays a minimum centered at 205 nm and a broad maximum at 227 nm. The origin of this maximum is unknown (*27*), but in any case, the spectrum

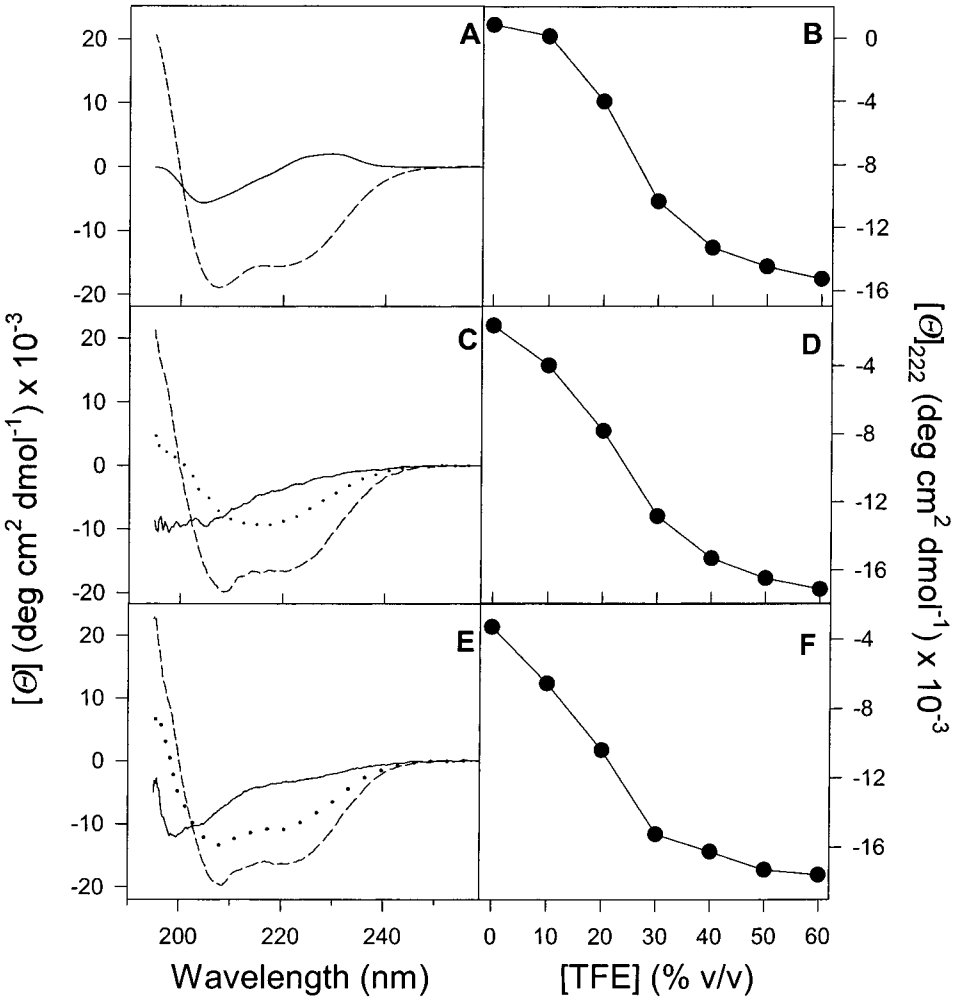

FIGURE 3: Effect of TFE on aFGF secondary structure. Panels A, C, and E display the far-UV CD spectra recorded in the presence of 0% (solid line), 20% (dotted line) and 60% (dashed line) TFE at pH 7.0, 4.0, and 2.0, respectively. The protein concentration was 7 μM. Panels B, D, and F show the variation of $[\theta]_{222}$ with TFE at pH 7.0, 4.0, and 2.0, respectively. The protein concentration in this case was 1.3 μM.

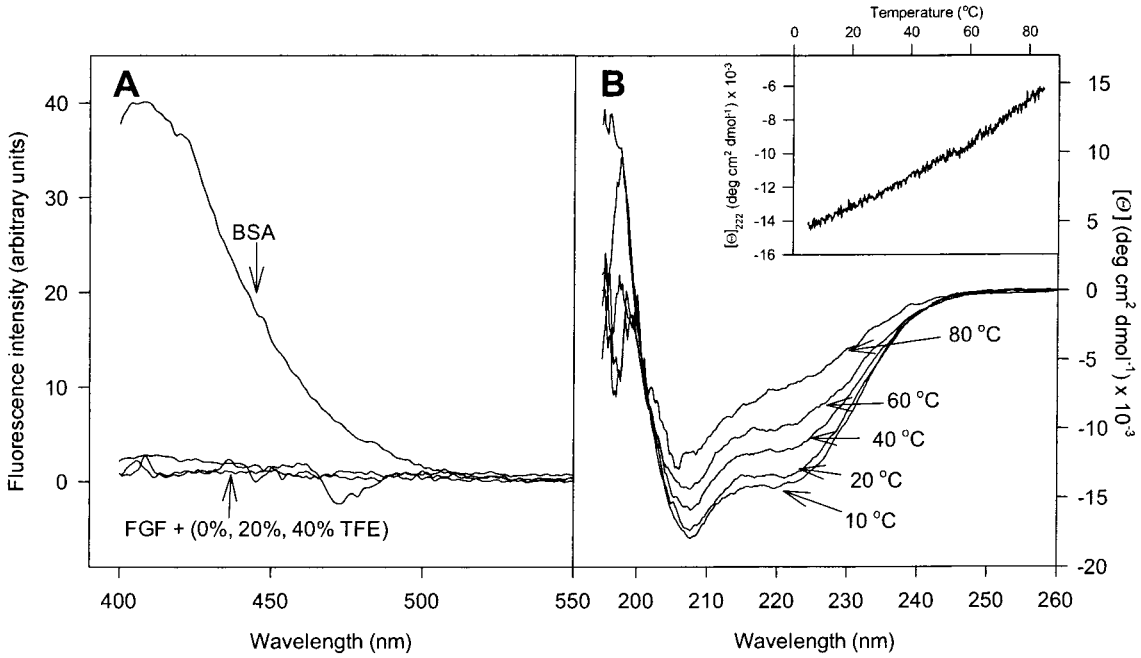

FIGURE 4: Hydrophobic cores of the TFE-induced state. Panel A: Fluorescence intensity of NPN added to bovine serum albumin (BSA) or aFGF at several TFE concentrations ([aFGF] = 1.3 μM). Panel B: Far-UV CD spectra of aFGF (7 μM) recorded at several temperatures in the presence of 60% TFE. Inset: variation of $[\theta]_{222}$ with temperature in these conditions.

does not reflect the content in secondary structure of aFGF [around 50% of antiparallel β-sheet (*25*)]. Addition of 60% TFE causes a change in the spectrum of the protein to one representative of α-helix, with two characteristic minima centered at 208 and 222 nm (Figure 3A). We observed precipitation between 20% and 30% TFE when the protein concentration was 0.1 mg/mL (7 μM), but a suitable titration could be carried out at 0.019 mg/mL (1.3 μM) protein using a 1 cm path-length cuvette without any visible aggregation (Figure 3B). However, we could not record the spectra below 215 nm in these conditions due to the high absorbance of the buffer (data not shown). In any case, we checked that there was no dependence of $[\theta]_{222}$ on protein concentration either in the absence or in the presence of 60% TFE (see below**)** so then we assumed that both sets of experiments using different protein concentrations are comparable. As shown in Figure 3B, the transition from the native to the TFE-induced state is cooperative, with a midpoint at 24% TFE and a final $[\theta]_{222}$ of -15250 deg cm^2 dmol^{-1}, that corresponds to 38% α-helix according to Rohl et al. (*28*). The cooperativity of the transition, achieved with a relatively low amount of TFE, suggests a high degree of specificity on helix induction. On the other hand, we observed that 500 μM heparin protected aFGF against TFE denaturation since a higher amount of the cosolvent was needed to induce the transition (data not shown).

We were not able to find conditions ensuring a complete refolding of aFGF upon removal of 60% TFE. The native CD spectrum is only partially recovered, and the mitogenic activity of the protein drops to 40% (data not shown). Due to this lack of full reversibility, we decided not to analyze the TFE-induced transitions in terms of equilibrium thermodynamics.

At pH 4, the transition is biphasic when a protein concentration of 7 μM is used. Figure 3C suggests an antiparallel β-sheet spectrum at 20% TFE that changes to an α-helical shape upon increasing the concentration of the alcohol. This biphasic behavior disappeared when the protein was titrated at a concentration of 1.3 μM (Figure 3D), which suggests that the formation of β-sheet-containing partially folded states of aFGF at intermediate concentrations of TFE is an intermolecular event that might also happen at pH 7, leading to visible precipitation. On the other hand, the titration at pH 2 was found to be independent of protein concentration, and no formation of β-structures or aggregates was detected. As depicted in Figure 3E,F, helix formation is favored at low pH (reaching 55%), needing a smaller TFE concentration.

Characterization of the Helical State of aFGF. As shown above, aFGF possesses extensive α-helical secondary structure at pH 7.0 in the presence of >40% TFE (Figure 3A,B). The tertiary structure of proteins is usually estimated by monitoring the environment of the aromatic side chains by near-UV CD spectroscopy. However, the near-UV CD signal of aFGF is very weak (data not shown). For these reasons, the three-dimensional packing of the TFE-induced helical state of aFGF was assessed by checking the state of the hydrophobic cores of the protein. Solvent-accessible apolar patches of proteins can be probed by the change in fluorescence of small, hydrophobic molecules such as 1-anilino-8-naphthalenesulfonic acid (ANS) (*48*). However, the structural similarities of ANS with other sulfated ligands of aFGF such as heparin or *myo*-inositol hexasulfate prompted us to use instead an analogue probe such as *N*-phenyl-1-naphthylamine (NPN), lacking the $-SO_3^-$ group (*49*). We had previously observed that NPN does not bind to the native state of aFGF at pH 7, suggesting a poor accesibility of the hydrophobic core to the solvent, although some binding could be observed at pH 2 (*27*). On the other hand, as expected, NPN interacts with bovine serum albumin (Figure 4A), a protein that binds apolar ligands. Induction of α-helix in aFGF by TFE could similarly expose the hydrophobic regions of the protein. However, no binding of NPN was observed at any TFE concentration at pH 7 (Figure 4A),

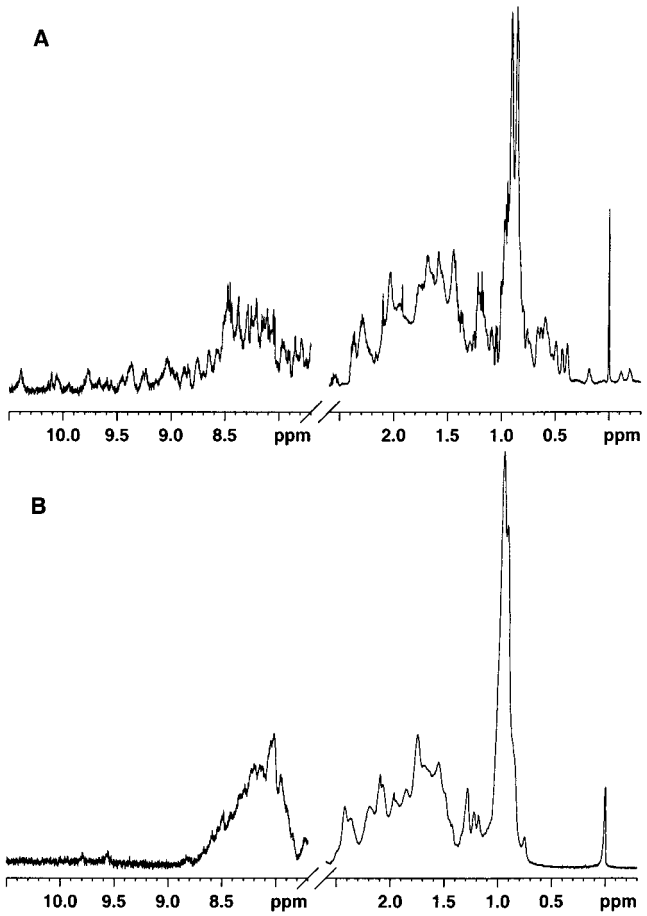

FIGURE 5: Selected regions of the 1D ^{1}H NMR spectra of aFGF (A) in 10 mM phosphate buffer, pH 6.0, and 9:1 H_2O/D_2O at 25 °C and (B) in 10 mM phosphate buffer, pH 6.0, and 40:60 (v/v) H_2O/TFE at 25 °C.

suggesting either that the protein is equally compact in the helicoidal state or, more likely, that the tertiary structure is disrupted. This point is confirmed by studying the thermal denaturation of the TFE-induced state of aFGF monitored by far-UV CD (Figure 4B). The loss of the CD signal at 222 nm is linear upon increasing the temperature (Figure 4B and inset). This result is not expected for a protein with a defined hydrophobic core, which would show a cooperative unfolding transition. The induction of α-helix on aFGF by TFE seems then to be accompanied by extensive unfolding of the tertiary packing of the protein.

The 1D ^{1}H NMR spectrum of aFGF in the presence of TFE (Figure 5) provides additional support about the lack of tertiary structure. The absence of signals at $\delta < 0.7$ ppm in contrast to the large number of these signals observed in aFGF in the native state and the fact that the large dispersion of the amide protons found in native aFGF is drastically reduced in the presence of TFE where these protons are clustered between 7.8 and 8.8 ppm confirms the absence of a well-defined tertiary structure.

Helical Propensity of β8 and β8/9 Peptides. As shown above (Figure 1), the sequence 95−104, corresponding to β-strand 8 is predicted as α-helical by five different prediction methods. To analyze the real propensity of β-strand 8 and the hairpin β8/β9 of aFGF, we synthesized the peptides corresponding to the 95−107 and 95−114 sequences as described in Experimental Procedures. We decided to change the residue Cys-97 to Ala in order to avoid complications due to the thiol group. A mutation to serine was discarded, as it has been described that such substitution causes a modification in the activity and stability of aFGF (*50*). An α-helical prediction on isolated peptides can be achieved by the AGADIR algorithm developed by Muñoz and Serrano (*45*). This program predicts for β8 an average helicity of 2.2% in water at pH 7 and 25 °C, which is significantly higher than the prediction for the fragments corresponding to the rest of the β-strands (a maximum of 0.28%, predicted for β12). AGADIR also calculates a higher content in α-helix for β8 at low pH (3.5%), most probably due to the protonation of the glutamic acid residues that would overcome any charge−charge repulsions in the helix. A per residue calculation of the helix content is shown in Figure 1.

The far-UV CD spectra of purified β8 peptide at different pH and TFE concentrations are shown in Figure 6, and some relevant data are displayed in Table 1. According to CD, the peptide is predominantly in a random coil conformation at pH 7 (Figure 6A). Addition of TFE (Figure 6A) induces a change toward a clear α-helical structure (51%) in a cooperative fashion and in a relatively low TFE concentration (midpoint at 20%; Figure 6B). The helical propensity is strongly favored at pH 2 so that the peptide is already 30% helical in the absence of TFE (Figure 6C, Table 1), and the conformational change is complete at 20% TFE (Figure 6D), reaching a final value of 76% α-helix (Table 1). We did not observe any dependence of the CD spectra with the peptide concentration within the micromolar to millimolar range (data not shown). The transitions at pH 7 and 2 display isodichroic points at 203 and 202 nm, respectively (Figure 6), and were fully reversible (data not shown). This prompted us to analyze the curves by two-state equilibrium thermodynamics according to the binding-exchange model of Jasanoff and Fersht (*29*) using eq 1, which yields an m value of 27.00 ± 1.47 kcal mol^{-1} and a transition midpoint $([TFE]/[H_2O])_{1/2}$ of 0.050 ± 0.001 at pH 7. The associated free energy change ($\Delta G°$) is 1.38 ± 0.33 kcal mol^{-1}. The data obtained at pH 2 were not analyzed due to the lack of a reliable pretransition baseline. In the case of peptide β8/9, the helical content observed at pH 7.0 and 2.0 in the presence of 60% TFE raises to 67% and 72%, respectively (Figure 7, Table 1), i.e., a percent amount of α-helix similar or even higher than that of β8. Given the longer length of β8/9, then the absolute amount of residues with helical conformation should be also higher in β8/9. The addition of residues 108−114 to the 95−107 sequence might give rise to two possible phenomena: (i) the number of helical residues in the 95−107 sequence does not change, but the total helical population increases, or (ii) the α-helix is elongated in the C-terminus. Fitting the β8/9 data shown in Figure 7B to eq 2 yields a transition midpoint $([TFE]/[H_2O])_{1/2}$ of 0.059 ± 0.002 with an m value of 39.92 ± 4.90 kcal mol^{-1} and $\Delta G° = 2.36 \pm 1.19$ kcal mol^{-1}. Interestingly, the m value for the TFE titration of β8/9 is 1.48 times higher than that for β8, and according to Jasanoff and Fersht (*29*), the value of m for related peptides increases with the helix length, possibly linearly. With these results in mind, we are tempted to predict that the addition of residues 108−114 induces the elongation of the α-helix formed in the 95−107 sequence.

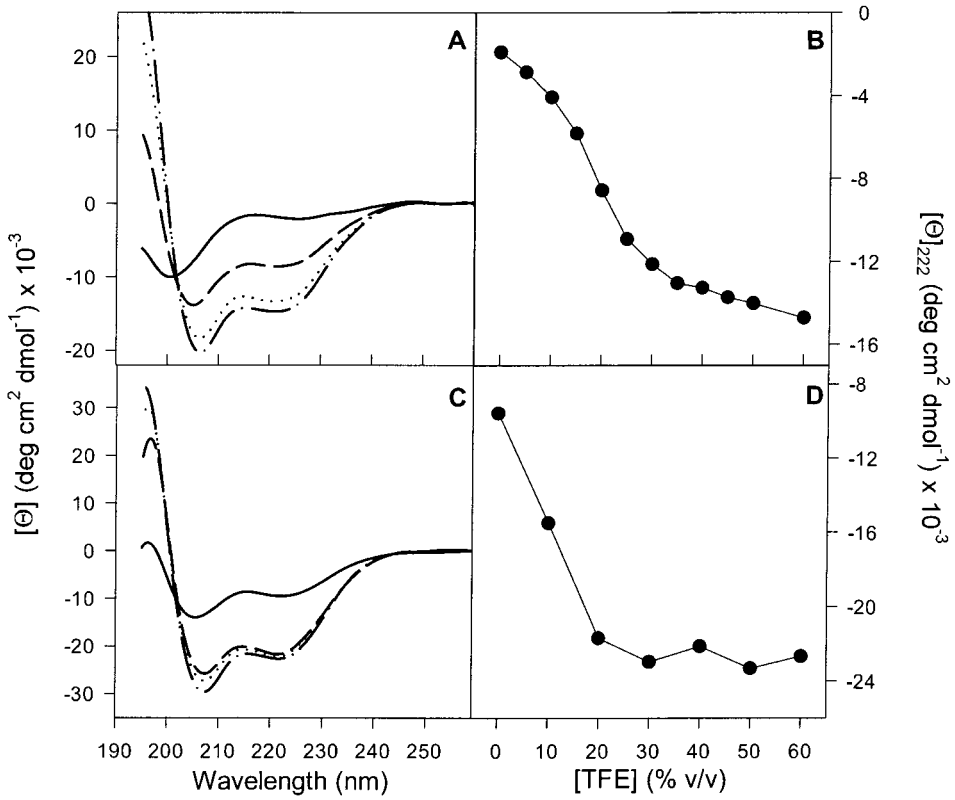

FIGURE 6: TFE titration of the β8 peptide. Panels A and C: far-UV CD spectra of the β8 peptide (7 μM) in the presence of 0% (solid line), 20% (dashed line), 40% (dotted line), and 60% (dashed−dotted line) TFE at pH 7.0 and 2.0, respectively. Panels B and D: variation of $[\theta]_{222}$ with [TFE] at pH 7.0 and 2.0, respectively.

Table 1: Effect of Additives on the Secondary Structure of β8 and β8/9 Peptides

		$[\theta]_{222}$ (deg cm^2 dmol^{-1})		% helical content[b]	
pH	addition[a]	β8	β8/9	β8	β8/9
7.0	none	−2610	−2680	12	11
7.0	60% TFE	−14730	−21720	51	67
7.0	25% methanol	−3920	−5960	16	21
7.0	50 mM SDS	−5970	−6740	23	23
2.0	none	−8080	−7775	30	26
2.0	60% TFE	−22680	−23340	76	72

[a] The sample is dissolved in all cases in 50 mM sodium phosphate buffer, pH 7.0, plus 50 mM NaCl or 50 mM glycine, pH 2.0, plus 50 mM NaCl. [b] According to eq 1.

The pH-induced conformational change of the β8 and β8/9 peptides in the absence of TFE was monitored by CD as shown in Figure 8. The transitions are sigmoidal and reversible and independent of the ionic strength up to 500 mM NaCl (data not shown). We analyzed the curves using eq 3 (*30*), according to which roughly 1 proton (0.85 ± 0.05 for β8, 0.93 ± 0.07 for β8/9) is taken up with an equivalence midpoint of 4.21 ± 0.04 for β8 and 4.22 ± 0.04 for β8/9. Therefore, these results suggest that the coil−helix transition of both peptides in the absence of TFE is driven by the protonation of one out of the five glutamate residues in the peptides. Interestingly, no significant variation of the CD signal can be seen around pH 6, suggesting that the protonation state of His-107 does not affect the helical propensity of the peptides.

The results presented so far indicate a clear α-helical tendency of the 95−114 sequence of aFGF at low pH or in the presence of TFE. Moreover, as depicted in Table 1, other compounds such as 25% methanol and SDS micelles (50 mM) were also successful in inducing α-helix in the peptide, although to a lesser degree. We also analyzed the effect of liposomes on the conformation of the β8 peptide. We found that, at pH 4.0, small unilamellar vesicles made of 0.25 mg/mL dimyristoylglycerophosphocholine also potentiated the helical content of β8 ($[\theta]_{222} = -11020$ deg cm^2 dmol^{-1}, 39% α-helix) (data not shown).

Despite the fact that the sequence 95−114 is in extended conformation in native conditions, forming a β-hairpin (Figure 2), we could not find any conditions that simulated the environment of the peptide in the folded state of aFGF so that the peptide could achieve a β-strand conformation, as described for other peptides (*14*): neither detergents such as 0.5 mM and 5 mM deoxycholate, 50 mM octyl glucoside, or SDS in submicellar concentrations (<8 mM) nor other agents such as 50% glycerol, 20% acetonitrile, or 1 M saccharose exerted any effect on the structure of β8 or β8/9 (data not shown). Some authors have been able to switch between helicoidal and extended conformations by changing the temperature (*51*). However, upon heating of the β8 and β8/9 fragments to 85 °C, which produced a linear decrease in the intensity of the CD signal, and subsequently cooling of the samples, the recovered CD spectrum was virtually identical to the initial both in the absence and presence of TFE at pH 2 and 7 (data not shown).

NMR Conformational Study. 2D ^{1}H NMR methods were used to investigate with deeper detail the conformational properties of peptides β8 and β8/9 at low pH. Conformational behavior of peptide β8 was studied in aqueous solution and in 30% TFE solution. That of peptide β8/9, however, could be only analyzed in 30% TFE solution because of its insolubility in water at the NMR concentrations.

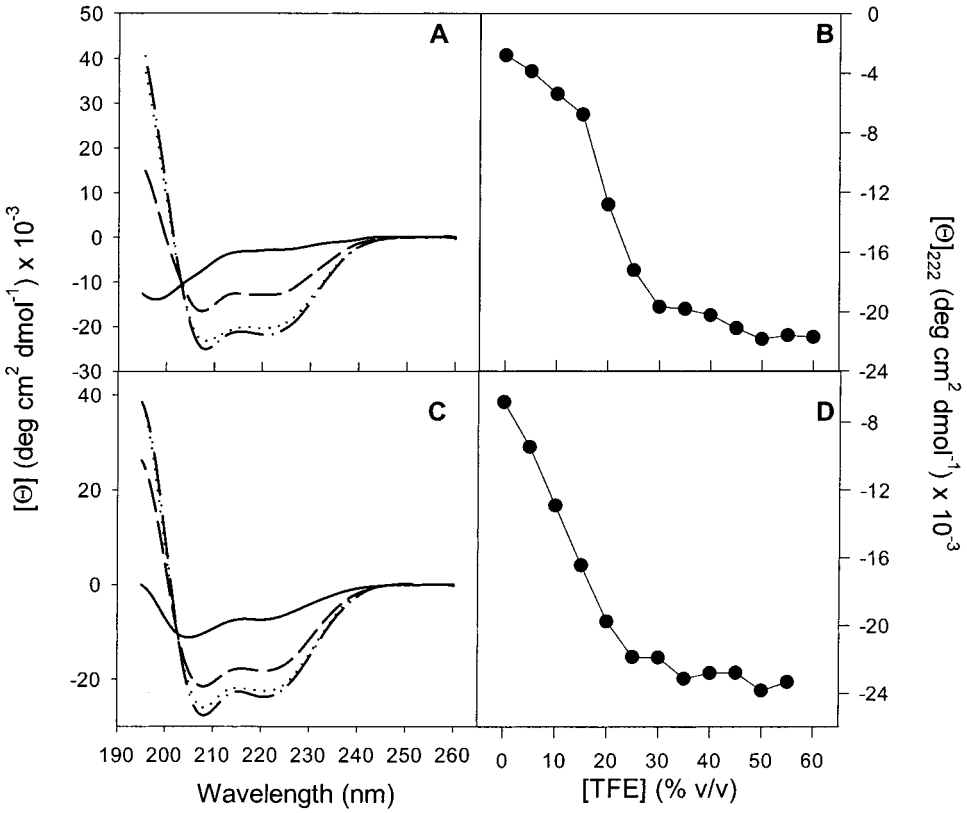

FIGURE 7: TFE titration of the β8/9 peptide. Panels A and C: far-UV CD spectra of the β8/9 peptide (7 μM) in the presence of 0% (solid line), 20% (dashed line), 40% (dotted line), and 60% (dashed−dotted line) TFE at pH 7.0 and 2.0, respectively. Panels B and D: variation of $[\theta]_{222}$ with [TFE] at pH 7.0 and 2.0, respectively.

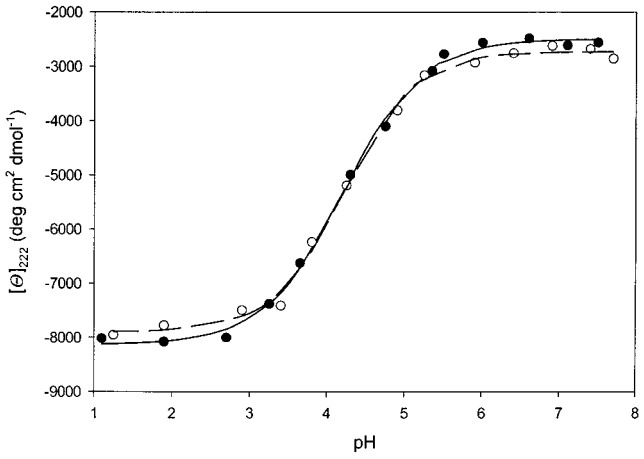

FIGURE 8: pH titration of peptides β8 and β8/9. The graph displays the variation of $[\theta]_{222}$ with pH for β8 (●) and β8/9 (○), together with the fittings to eq 3, (—) and (- - -), respectively.

^{1}H NMR spectra were assigned by using standard two-dimensional sequence-specific methods (*52*, *53*) (data available in Supporting Information). The sequential NN, αN, and βN NOE connectivities used for assignment are summarized in Figure 9. Several NMR parameters provide information on the structural features of peptides. The most conclusive evidence about the existence of preferred structures in peptides comes from the NOE connectivities, in particular from the nonsequential ones. The pattern of nonsequential NOEs allows to identify the type of secondary structure. Thus, stretches of $d_{\alpha Ni,i+2}$, $d_{\alpha Ni,i+3}$, $d_{\alpha Ni,i+4}$, $d_{\alpha\beta i,i+3}$, and $d_{NNi,i+2}$ NOE connectivities are characteristic of helices (*53*). The deviations of the δ values measured for the CαH protons in a peptide with respect to those expected for nonstructured peptides [conformational $\Delta\delta_{C\alpha H}$ shifts, $\Delta\delta = \delta_{observed} - \delta_{RC}$ (ppm)] provide additional information about the presence and nature of the preferred conformation adopted by a peptide. These deviations are negative in helices and positive in extended or β-sheet conformations (*54*, *55*). The NOE connectivities observed for β8 in aqueous and in 30% TFE solutions and that of peptide β8/9 in 30% TFE solution are summarized in Figure 9. Apart from the sequential NOE connectivities used for assignment, nonsequential NOE cross-peaks were also observed for peptide β8 in aqueous solution. They are a stretch of $d_{\alpha\beta i,i+3}$, characteristic of helices, and a few nonsequential $i,i+3$ and $i,i+4$ NOE connectivities involving side chain protons which are also compatible with the formation of helical structures. The negative and large in absolute value ($|\Delta\delta| > 0.1$ ppm) conformational $\Delta\delta_{C\alpha H}$ shifts found for residues 97−103 and 106 (Figure 9A) again indicate the formation of a helical structure. In 30% TFE solution, the number of nonsequential NOEs observed for peptide β8, all of them indicative of a helical structure, increases, and the conformational $\Delta\delta_{C\alpha H}$ shifts become more negative (Figure 9B). This indicates an increment of the helix population in the presence of 30% TFE, in agreement with the CD data. Taking into account nonsequential NOEs and conformational $\Delta\delta_{C\alpha H}$ shifts, the helix spans residues 96−106 in aqueous solution and residues 95−106 in 30% TFE solution. The population of the helix adopted is about 40% and 59% in aqueous solution and 30% TFE, respectively, as estimated from the averaged $\Delta\delta$ of the CαH within the helical region 95−106 (*41*−*43*). The set of NOE connectivities observed for peptide β8/9 in 30% TFE, which contains long stretches of $d_{\alpha Ni,i+3}$, $d_{\alpha Ni,i+4}$, $d_{\alpha\beta i,i+3}$, and $d_{NNi,i+2}$ NOEs (Figure 9C), is characteristic of an α-helix.

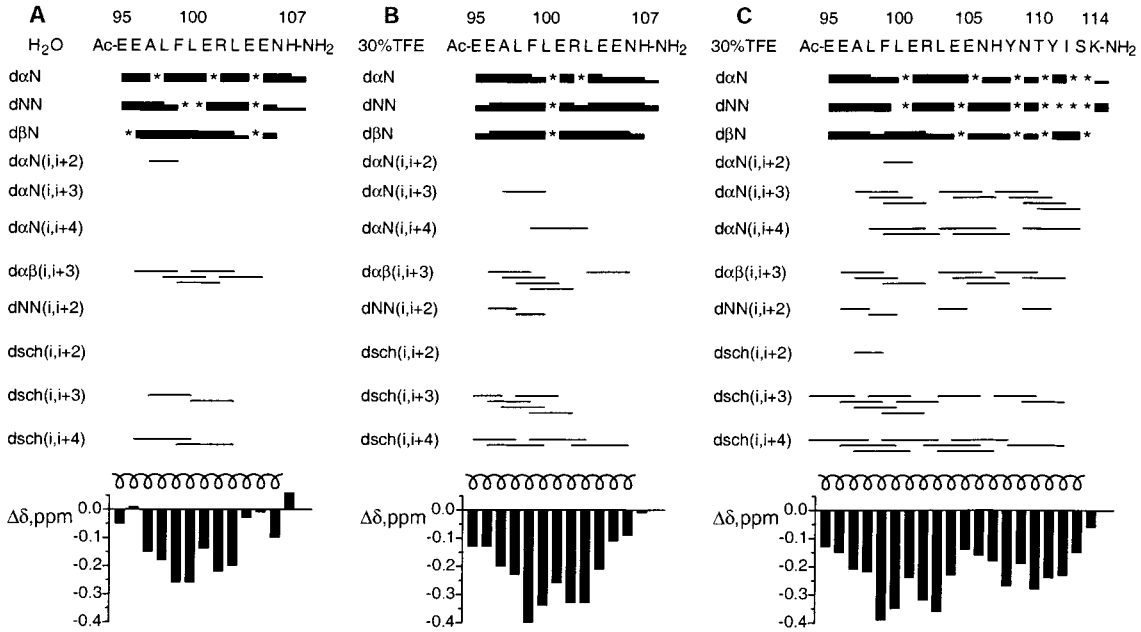

FIGURE 9: NMR experiments on peptides β8 and β8/9. Summary of NOE connectivities, secondary structure, and conformational $\Delta\delta_{C\alpha H}$ shifts [$\Delta\delta_{C\alpha H} = \delta_{C\alpha H(observed)} - \delta_{C\alpha H(random\ coil)}$ (ppm), where $\delta_{C\alpha H(random\ coil)}$ are the δ values corresponding to random coil peptides (*38*)] observed for peptide β8 in 20 mM phosphate buffer at pH 2.0 and 20 °C (A) and in 30% TFE at pH 2.0 and 20 °C (B) and for peptide β8/9 in 30% TFE at pH 2.0 and 20 °C (C). The thickness of the lines reflects the intensity of the sequential NOE connectivities, i.e., weak, medium, and strong. An asterisk (*) indicates unobserved NOE connectivity due to signal overlapping, closeness to diagonal, or overlapping with solvent signal. NOE conectivities involving side chains are indicated by dsch.

The negative and large in absolute value ($\Delta\delta > 0.1$ ppm) conformational $\Delta\delta_{C\alpha H}$ shifts observed for residues 95−113 confirm the formation of helix. Thus, NMR data clearly indicate that peptide β8/9 adopts a helix spanning residues 95−113 in 30% TFE. The population estimated from the averaged $\Delta\delta$ of the CαH within this helical region was about 58% (*56*−*58*).

DISCUSSION

Experimental and theoretical evidence has led to the formulation of different protein folding models (*2*, *5*, *6*) which mainly differ in the sequence of events that occur in the folding process. Nevertheless, it seems difficult for a unique model to include all experimental data (sometimes apparently conflicting), and for a particular case one particular model may give a better explanation than the others. The study of all-β proteins complicates this panorama, although any complete folding model must aim to explain the folding of this type of polypeptide. Acidic fibroblast growth factor belongs to the all-β family and is a good candidate for folding studies, since its three-dimensional structure is known (*21*, *23*−*25*) and is accessible to protein engineering manipulation.

The prediction of the secondary structure of aFGF by several procedures (Figure 1) identifies most of the residues in the correct conformation. Most of the mismatches occur in the β-sheet edges. The prediction for the sequences corresponding to β-strands 3 and 11 yields a somewhat higher preference for the coil conformation. Interestingly enough, the sequence of β-strand 8 is unequivocally predicted as α-helical by five out of the seven methods used. Therefore, the possibility existed that some sequences of aFGF had a local propensity that might vary substantially when inserted into the context of the folded protein, as described for the "chamaleon sequence" of Minor and Kim (*15*) or for β-lactoglobulin (*12*). The model of nonhierarchical folding, described by several groups (*12*, *59*), suggests that folding is initiated on the basis of local (short-range) propensities, so that in some cases segments of non-native structure may form. As folding proceeds, the new environment created by the preformed tertiary structure may force such non-native structures to change their conformation (*60*).

We analyzed the helical propensity of aFGF in the presence of trifluoroethanol (TFE). TFE is known to increase the local propensities of peptides by stabilizing the α-helical conformation in the majority of cases, although this solvent can also stabilize β-turns and β-hairpins (ref *29* and citations therein). Moreover, TFE has also been found to stabilize non-native α-helices (*12*, *61*, *62*) and to induce, at high concentrations (around 80%), α-helical character to charged homopolypeptides at neutral pH, when they are supposed to exist in random coil conformation (*63*). Before proceeding with the discussion, we must ensure that our approach in using TFE for analyzing "true" propensities is valid. According to Buck (*47*), TFE is a worse hydrogen bond partner than water, promoting intramolecular bonds within the polypeptide chain. Moreover, since TFE has a low dielectric constant, such hydrogen bonds are strengthened; finally, TFE/H_2O mixtures are more hydrophobic than pure H_2O and then the hydrophobic groups of the protein are better solvated. Therefore, these conditions might mimic the early steps of folding, where long-range tertiary interactions are absent and local interactions are dominant. The specificity of TFE is given by the cooperativity of the transition induced by the solvent as well as by the concentrations used; i.e., a very cooperative transition occurring in a relatively low percentage of TFE (<40%) is very likely to be specific (*61*). Higher concentrations of TFE may affect the pK_a of charged residues, as probably happens with polyglutamate or polylysine peptides at neutral pH (*63*). Those sequences with little helical propensity will need higher amounts of TFE, form

less α-helix noncooperatively, or form no α-helix at all (*12*, *64*).

aFGF acquires 40% α-helix in the presence of TFE at neutral pH (Figure 3). The titration is cooperative and occurs with a midpoint of 24% TFE at pH 7. The TFE-induced state lacks any detectable tertiary structure: it does not bind the hydrophobic probe NPN (Figure 4A), nor does it display a cooperative thermal unfolding transition (Figure 4B), indicating the absence of a defined hydrophobic core, which is confirmed by the broad, featureless 1D ^{1}H NMR spectrum shown in Figure 5. The amount of TFE-induced helix (38%) is clearly higher than predicted by any of the methods tested (15% at most; Figure 1). In this sense, Shiraki et al. (*12*) have found empirically that TFE stabilizes a somewhat higher helical content than predicted, although there is a neat linear relationship between the predicted and the experimental α-helical quantities for a number of proteins (see Figure 9 of ref *12*). According to the equations derived by these authors (eqs 4 and 5) and assuming a prediction of 15% helix, the $[\theta]_{222}$ value of aFGF in the presence of 40% TFE should be -16350 deg cm^2 dmol^{-1} at pH 2 and -12145 deg cm^2 dmol^{-1} at pH 7. These values are very similar to the experimental values of -16250 and -13250 deg cm^2 dmol^{-1} at pH 2 and 7, respectively (Figure 3).

It has previously been described that aFGF acquires at pH 4.0 a partially folded conformation which is very structured (*27*, *65*). This and the TFE-induced equilibrium intermediate of the protein might represent kinetic counterparts as there is increasing evidence of the equivalence between equilibrium and kinetic intermediates (*66*). This would confirm the hypothesis a nonhierarchical folding of the protein, in which the equilibrium conformations obtained in the presence of TFE or at pH 4.0 may resemble kinetic intermediates that occur very early and very late, respectively, in the folding process, with other intermediates in between. This hypothesis is attractive but must be clarified in the future with further experiments (see below). In any case, the acquisition of the native structure of aFGF is certainly a complex, multistep mechanism. Mach et al. (*65*) described the existence of a kinetic intermediate of aFGF that accumulates in the first 200 ms of folding and that binds the hydrophobic probe ANS. On the other hand, Samuel et al. (*67*) have recently claimed that a partially folded intermediate occurs in the folding pathway of aFGF as deduced from the noncoincidence of the fluorescence and CD stopped-flow time traces, as well as NMR quenched-flow experiments. Although no "overshoot" can be seen in the dead time of the stopped-flow experiments, the presence of kinetic helical intermediates cannot be completely ruled out as they are probably little populated (in fact, AGADIR prediction is never higher than 5% throughout the sequence; data not shown). In this case, addition of small amounts of TFE might help to stabilize the helical intermediate (should it exist) so that the kinetic overshoot could become more evident (see ref *9*). Moreover, a kinetic and thermodynamic analysis of aFGF mutants that decrease or increase the helix propensity of β-strand 8/turn/β-strand 9 hairpin could help to define the folding pathway of the protein in terms of non-native intermediates.

Kinetic intermediates have also been studied for other all-β proteins, such as the β-trefoiled human interleukin 1-β (*68*), whose structure is homologous to that of aFGF. In both cases, the intermediates display far-UV CD spectra characteristic of β-structure, although they are very flexible as deduced from NMR experiments. There are no signs of helical intermediates, but concomitantly their sequences show little, if any, propensity to form α-helix according to the programs used in this work (data not shown).

We can have an estimate of the early steps of folding of aFGF using peptide fragments of its sequence. The study of two peptides seems obvious: sequence 95−107, corresponding to β-strand 8, for which an α-helical conformation is predicted (Figure 1), and sequence 95−114, corresponding to β-hairpin 8/9, that contains β-strand 8 and that constitutes a loop relatively isolated from the rest of the protein (Figure 2). The AGADIR prediction confirms the helical tendency of the isolated 95−107 sequence (Figure 1). Although the β8 and β8/9 peptides are mostly unstructured at pH 7, TFE induces a high amount of helicity in a specific fashion, as the CD (Figures 6 and 7 and Table 1) and NMR (Figure 9) data demonstrate. The content in α-helix increases substantially upon decreasing the pH (Figure 8) due probably to the uptake of one proton by Glu101 or Glu105, which would lie in the same helix ridge: protonation of these residues would abolish any electrostatic repulsion between them. TFE is not the only agent affecting the structure of β8: methanol and SDS micelles (Table 1), as well as lipid vesicles, can stabilize the α-helix of β8. On the other hand, we have been unsuccessful in inducing β structure in both peptides.

Binding of heparin (the so-called "low-affinity receptor") protects aFGF against TFE denaturation. The binding site of the polysaccharide is located in the turn/β11/turn region spanning residues 126−142, through a network of van der Waals, electrostatic, and hydrogen bonds (*46*). This region is located at some distance of the β8/β9 hairpin. Upon binding of heparin or heparin analogues, the structure of aFGF is stabilized as a whole (*26*), so that a higher amount of any denaturant such as TFE is needed to unfold the protein. On the other hand, it is somewhat intriguing that the β8/β9 hairpin, the aFGF sequence with most helical propensity, belongs to the main patch recognized by the membrane cell receptor (*46*). It is possible that aFGF mutants that decrease or increase the helical propensity of the hairpin and do not modify the residues actively involved in binding might have an effect on the stability (and flexibility) of the hairpin and, accordingly, on the affinity to the receptor.

In summary, in this work we have compared the native structure of aFGF with the local propensity of its sequence. Despite being an all-β protein, some segments of aFGF are predicted as α-helical. Such segments have a tendency to form α-helix in solution when isolated. aFGF itself can form a helical intermediate state in equilibrium in the presence of moderate amounts of TFE, and this may represent an amplified model of an early kinetic folding intermediate. All of these results suggest that the folding of aFGF is nonhierarchical and that non-native intermediates, based in local propensities, may arise in the folding pathway. More studies on this subject need to be carried out since, if nonhierarchical mechanisms are widespread, it complicates the panorama of protein structure prediction because of the "folding feedback" concept (*14*): a reliable prediction of the native secondary structure of the protein needs paradoxically essential information of the tertiary structure, since the latter may change the local propensity of the sequence. This could explain why the best secondary structure prediction methods not based

in sequence similarities with proteins of known three-dimensional structure only achieve 70% success on average, suggesting that they might instead predict the structure of folding intermediates.

SUPPORTING INFORMATION AVAILABLE

One table giving chemical shifts of peptides β8/9 and β8 in 30% TFE. This material is available free of charge via the Internet at http://pubs.acs.org.

REFERENCES

1. Ptitsyn, O. B. (1987) *J. Protein Chem. 6*, 273−293.
2. Kim, P. S., and Baldwin, R. L. (1990) *Annu. Rev. Biochem. 59*, 631−660.
3. Kuwajima, K. (1989) *Proteins: Struct., Funct., Genet. 6*, 87−103.
4. Dill, K. A., Fiebig, K. M., and Chan, H. S. (1993) *Proc. Natl. Acad. Sci. U.S.A. 90*, 1942−1946.
5. Fersht, A. R. (1997) *Curr. Opin. Struct. Biol. 7*, 3−9.
6. Dill, K. A., and Chan, H. S. (1997) *Nat. Struct. Biol. 4*, 10−18.
7. Carlsson, U., and Jonsson, B.-H. (1995) *Curr. Opin. Struct. Biol. 5*, 482−487.
8. Liu, Z.-P., Rizo, J., and Gierasch, L. M. (1994) *Biochemistry 33*, 134−142.
9. Hamada, D., Segasa, S., and Goto, Y. (1996) *Nat. Struct. Biol. 3*, 868−873.
10. Kuwajima, K., Yamaya, H., and Sugai, S. (1996) *J. Mol. Biol. 264*, 806−822.
11. Hamada, D., and Goto, Y. (1997) *J. Mol. Biol. 269*, 479−487.
12. Shiraki, K., Nishikawa, K., and Goto, Y. (1995) *J. Mol. Biol. 245*, 180−194.
13. Hamada, D., Kuroda, Y., Tanaka, T., and Goto, Y. (1995) *J. Mol. Biol. 254*, 737−746.
14. Zhong, L., and Johnson, W. C., Jr. (1992) *Proc. Natl. Acad. Sci. U.S.A. 89*, 4462−4465.
15. Minor, D. L., and Kim, P. S. (1996) *Nature 380*, 730−734.
16. Thomas, P. J., Qu, B.-H., and Pedersen, P. L. (1995) *Trends Biochem. Sci. 20*, 456−459.
17. Carrell, R. W., and Lomas, D. A. (1997) *Lancet 350*, 134−138.
18. Giménez-Gallego, G., and Cuevas, P. (1994) *Neurol. Res. 16*, 313−316.
19. Giménez-Gallego, G., Conn, G., Hatcher, V., and Thomas, K. A. (1986) *Biochem. Biophys. Res. Commun. 135*, 541−548.
20. Yayon, A., Klagsbrun, M., Esko, J. D., Leder, P., and Ornitz, D. M. (1991) *Cell 64*, 841−848.
21. Pineda-Lucena, A., Jiménez, M. A., Nieto, J. L., Santoro, J., Rico, M., and Giménez-Gallego, G. (1994) *J. Mol. Biol. 242*, 81−98.
22. Burgess, W. H., and Maciag, T. (1989) *Annu. Rev. Biochem. 58*, 575−606.
23. Zhu, X., Komiya, H., Chirino, A., Faham, S., Fox, G. M., Arakawa, T., Hsu, B. T., and Rees, D. C. (1991) *Science 251*, 90−93.
24. Romero, A., Pineda-Lucena, A., and Giménez-Gallego, G. (1996) *Eur. J. Biochem. 241*, 453−461.
25. Pineda-Lucena, A., Jiménez, M. A., Lozano, R. M., Nieto, J. L., Santoro, J., Rico, M., and Giménez-Gallego, G. (1996) *J. Mol. Biol. 264*, 162−178.
26. Murzin, A. G., Lesk, A. M., and Chothia, C. (1992) *J. Mol. Biol. 223*, 531−543.
27. Sanz, J. M., and Giménez-Gallego, G. (1997) *Eur. J. Biochem. 246*, 328−355.
28. Rohl, C. A., and Baldwin, R. L. (1997) *Biochemistry 36*, 8435−8442.
29. Jasanoff, A., and Fersht, A. R. (1994) *Biochemistry 33*, 2129−2135.
30. Oliveberg, M., Vuilleumier, S., and Fersht, A. R. (1994) *Biochemistry 33*, 8826−8832.
31. Aue, W. P., Bartholdi, E., and Ernst, R. R. (1976) *J. Chem. Phys. 64*, 2229−2246.
32. Bax, A., and Davis, D. G. (1985) *J. Magn. Reson. 65*, 355−360.
33. Kumar, A., Ernst, R. R., and Wüthrich, K. (1980) *Biochem. Biophys. Res. Commun. 95*, 1−6.
34. Bothner-By, A. A., Stephens, R. L., Lee, J. M., Warren, C. D., and Jeanloz, R. W. (1984) *J. Am. Chem. Soc. 106*, 811−813.
35. Braunschweiler, L., and Ernst, R. R. (1983) *J. Magn. Reson. 53*, 521−528.
36. Redfield, A. G., and Kuntz, S. D. (1975) *J. Magn. Reson. 19*, 250−254.
37. Rance, M. (1987) *J. Magn. Reson. 74*, 557−564.
38. King, R. D., and Sternberg, M. J. (1996) *Protein Sci. 5*, 2298−2310.
39. Garnier, J., Gibrat, J. F., and Robson, B. (1996) *Methods Enzymol. 266*, 540−553.
40. Guermeur, Y., Geourjon, C., Gallinari, P., and Deleage, G. (1999) *Bioinformatics 15*, 413−421.
41. Rost, B., and Sander, C. (1994) *Proteins 19*, 55−72.
42. Frishman, D., and Argos, P. (1996) *Protein Eng. 9*, 133−142.
43. Levin, J. (1997) *Protein Eng. 7*, 771−776.
44. Geourjon, C., and Deleage, G. (1995) *Comput. Appl. Biosci. 11*, 681−684.
45. Muñoz, V., and Serrano, L. (1997) *Biopolymers 41*, 495−509.
46. Pellegrini, L., Burke, D. F., von Delft, F., Mulloy, B., and Blundell, T. L. (2000) *Nature 407*, 1029−1034.
47. Buck, M. (1998) *Q. Rev. Biophys. 31*, 297−355.
48. Semisotnov, G. V., Rodionova, N. A., Razgulyaev, O. I., Uversky, V. N., Gripas, A. F., and Gilmanshin R. I. (1991) *Biopolymers 31*, 119−128.
49. Pala, I., Vig, P. J., Desaiah, D., and Srinivasan, A. (1991) *J. Appl. Toxicol. 11*, 391−395.
50. Ortega, S., Schaeffer, M. T., Soderman, D., DiSalvo, J., Linemeyer, D. L., Gimenez-Gallego, G., and Thomas, K. A. (1991) *J. Biol. Chem. 266*, 5842−5846.
51. Cerpa, R., Cohen, F. E., and Kuntz, I. D. (1996) *Folding Des. 1*, 91−101.
52. Wüthrich, K., Billeter, M., and Braun, W. (1984) *J. Mol. Biol. 180*, 715−740.
53. Wüthrich, K. (1986) *NMR of Proteins and Nucleic Acids*, J. Wiley and Sons, New York.
54. Wishart, D. S., and Sykes, B. D. (1994) *Methods Enzymol. 239*, 363−392.
55. Case, D. A., Dyson, H. J., and Wright, P. E. (1994) *Methods Enzymol. 239*, 392−416.
56. Jiménez, M. A., Bruix, M., González, C., Blanco, F. J., Nieto, J. L., Herranz, J., and Rico, M. (1993) *Eur. J. Biochem. 211*, 569−581.
57. Jiménez, M. A., Muñoz, V., Rico, M., and Serrano, L. (1994) *J. Mol. Biol. 242*, 487−496.
58. Rizo, J., Blanco, F. J., Kobe, B., Bruch, M. D., and Gierasch, L. M. (1993) *Biochemistry 32*, 4881−4894.
59. Chikenji, G., and Kikuchi, M. (2000) *Proc. Natl. Acad. Sci. U.S.A. 97*, 14273−14277.
60. Cregut, D., Civera, C., Macias, M. J., Wallon, G., and Serrano, L. (1999) *J. Mol. Biol. 292*, 389−401.
61. Sönnichsen, F. D., van Eyk, J. E., Hodges, R. S., and Sykes, B. D. (1992) *Biochemistry 31*, 8790−8798.
62. Schönbrunner, N., Wey, J., Engels, J., Georg, H., and Kiefhaber, T. (1996) *J. Mol. Biol. 260*, 432−445.
63. Arunkumar, A. I., Kumar, T. K. S., and Yu, C. (1997) *Biochim. Biophys. Acta 1338*, 69−76.
64. Dyson, H. J., Sayre, J. R., Merutka, G., Shin, H.-C., Lerner, R. A., and Wright, P. E. (1992) *J. Mol. Biol. 226*, 819−835.
65. Mach, H., Ryan, J. A., Burke, C. J., Volkin, D. B., and Middaugh, C. R. (1993) *Biochemistry 32*, 7703−7711.
66. Sanz, J. M., and Fersht, A. R. (1993) *Biochemistry 32*, 13584−13592.
67. Samuel, D., Kumar, T. K., Balamurugan, K., Lin, W. Y., Chin, D. H., and Yu, C. (2001) *J. Biol. Chem. 276*, 4134−4141.
68. Varley, P., Gronenborn, A. M., Christensen, H., Wingfield, P. T., Pain, R. H., and Clore, G. M. (1993) *Science 260*, 1110−1113.

BI0157619